

A Theoretical Investigation of the Remarkable Nuclear Spin–Spin Coupling Pattern in $[(\text{NC})_5\text{Pt–Tl}(\text{CN})]^-$

Jochen Autschbach*[†] and Tom Ziegler*[‡]

Contribution from the Department of Chemistry, The University of Calgary, Alberta T2N 1N4, Canada

Received November 3, 2000. Revised Manuscript Received January 8, 2001

Abstract: We address the problem of the interpretation of heavy nucleus spin–spin couplings for systems being studied in solution. Solvation can create counterintuitive features concerning the spin–spin couplings, which are enhanced by relativistic effects due to the presence of heavy nuclei. This should therefore be taken into consideration for the discussion of spectra obtained from solution. Evidence for such solvent effects is provided by a relativistic density functional study of $[(\text{NC})_5\text{Pt–Tl}(\text{CN})]^-$ (**1**). It is demonstrated that the remarkable experimentally observed spin–spin coupling pattern, e.g., ${}^2J(\text{Tl–C}) \gg {}^1J(\text{Tl–C})$ and $J(\text{Pt–Tl}) \sim 57$ kHz, is semiquantitatively reproduced by our calculations if both relativistic effects and solvation are taken into account. Solvent effects are very substantial and shift the Pt–Tl coupling by more than 100%, e.g. Relativistic increase of s-orbital density at the heavy nuclei, charge donation by the solvent, and the specific features of the multicenter C–Pt–Tl–C bond are responsible for the observed coupling pattern.

1. Introduction

Nuclear magnetic resonance (NMR) spectroscopical parameters involving heavy elements are of considerable experimental and theoretical interest.^{1–4} In particular, systems with direct metal–metal bonds quite often afford very large spin–spin coupling constants between metal centers. This is usually attributed to relativistic effects in the valence shell of the heavy atoms.⁵ However, the detailed mechanisms which determine the experimental output are not clear in many cases, and a very unsystematic behavior of Pt–Pt couplings, e.g., has been observed experimentally without explanation.⁶ Theoretical investigations are necessary in this case to clarify details about bonding in these systems. The accurate computation of heavy atom spin–spin couplings is a challenging task, though, e.g., a variational four-component ab initio implementation for nuclear spin–spin couplings at the Hartree–Fock level has been reported only recently,⁷ yielding rather large deviations compared with experiment for plumbanes due to the missing treatment of electron correlation. We have previously shown^{8,9}

that substantially improved accuracy for heavy atom spin–spin couplings can be achieved by employing a two-component relativistic density functional (DFT) method. Compared to a four-component method, the computational cost is kept rather low, in particular when spin–orbit coupling effects can be neglected (i.e., at a scalar relativistic “one-component” level).

A large amount of experimental NMR data for heavy atom compounds has been obtained from solution, and conclusions and accompanying interpretations of these data are therefore based on spectra which are more or less strongly influenced by solvation. Recently, we have studied solvent effects on spin–spin coupling constants for coordinatively unsaturated Hg and Pt complexes.¹⁰ While solvent effects were demonstrated to be very substantial and therefore necessary to yield quantitatively correct metal–ligand coupling constants and correct qualitative interpretations of experimental results comparing solvent-coordinated and -uncoordinated particles, they did not change the *qualitative* features of coupling patterns in the individual systems. However, in this work we want to point out that solvent coordination effects can be of such importance for nuclear spin–spin couplings that even counterintuitive results may occur. Successful attempts to explain experimentally observed coupling patterns therefore rely on the *awareness* of the possible consequences of solvation. We will demonstrate this in the following by a theoretical study of a striking example. This paper is also an extension of our previous work in the sense that we can demonstrate that not only one-bond couplings but also couplings between atoms separated by more than one bond can be substantially influenced by solvent-coordination effects.

A note on “solvent effects” is appropriate here. As in ref 10, we study a coordinatively unsaturated heavy metal compound, where solvent molecules can directly coordinate to a heavy atom. Computationally, those solvent molecules which complete the first coordination shell are considered explicitly. Studies in which the solvent is treated implicitly as a polarizable continuum and thereby also represents the bulk of solvent (for example in

* Address correspondence to either author.

[†] E-mail: jochen@cobalt78.chem.ucalgary.ca.

[‡] E-mail: ziegler@chem.ucalgary.ca.

(1) *NMR of newly accessible nuclei*; Lazlo, P., Ed.; Academic Press: New York, 1983; Vols. 1 and 2.

(2) (a) Wrackmeyer, B.; Horchler, K. *Ann. Rep. NMR Spectrosc.* **1989**, 22, 249. (b) Pregosin, P. *Ann. Rep. NMR Spectrosc.* **1986**, 17, 285. (c) Wrackmeyer, B.; Contreras, R. *Ann. Rep. NMR Spectrosc.* **1992**, 24, 267.

(3) Pyykkö, P. *Theor. Chem. Acc.* **2000**, 103, 214.

(4) Helgaker, T.; Jaszunski, M.; Ruud, K. *Chem. Rev.* **1999**, 99, 293.

(5) (a) Pyykkö, P.; Wiesenfeld, L. *Mol. Phys.* **1981**, 43, 557. (b) Jameson, J. C. In *Multinuclear NMR*; Plenum Press: New York, 1987.

(6) (a) Xu, Q.; Heaton, B. T.; Jacob, C.; Mogi, K.; Ichihashi, Y.; Souma, Y.; Kanamori, K.; Eguchi, T. *J. Am. Chem. Soc.* **2000**, 122, 6862. (b) Boag, N. M.; Goggin, P. L.; Goodfellow, R. J.; Herbert, I. R. *J. Chem. Soc., Dalton Trans.* **1983**, 1101. (c) Boag, M. N.; Browning, J.; Crocker, C.; Goggin, P. L.; Goodfellow, R. J.; Murray, M.; Spencer, J. J. *Chem. Res. (M)* **1978**, 2959.

(7) (a) Visscher, L.; Envoldsen, T.; Saue, T.; Jensen, H. J. A.; Oddershede, J. J. *Comput. Chem.* **1999**, 20, 1262. (b) Enevoldsen, T.; Visscher, L.; Saue, T.; Jensen, H. J. A.; Oddershede, J. J. *Chem. Phys.* **2000**, 112, 3493.

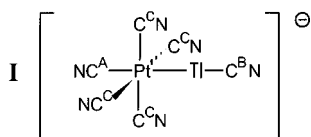
(8) Autschbach, J.; Ziegler, T. *J. Chem. Phys.* **2000**, 113, 936.

(9) Autschbach, J.; Ziegler, T. *J. Chem. Phys.* **2000**, 113, 9410.

(10) Autschbach, J.; Ziegler, T. *J. Am. Chem. Soc.* **2001**, 123, 3341.

ref 11) demonstrate that even very unspecific solvent effects can have nonnegligible contributions to the spin–spin couplings. This has been mainly attributed to the change of the molecular geometry upon solvation. We expect such solvent effects to further influence our results by typically some few percent. This is within the range of accuracy of the density functional method being used but is, of course, not at all negligible for computational results of high accuracy. However, the effect of direct coordination of a heavy atom by solvent molecules seems to be much larger and should be considered even at a qualitative level. The main influence on the spin–spin coupling for the samples studied in ref 10 results just from the close presence of the solvent, while the resulting change in geometry appears to influence the couplings much less.

Compounds which have a direct bond between two different heavy nuclei and which are stable in solution are rare. A class of such compounds, $[(NC)_5Pt-Tl(CN)]_n^{n-}$, $n = 0, \dots, 3$, with unbridged Pt–Tl bonds has been described by Glaser and co-workers.^{12,13} These complexes have also been studied computationally very recently concerning their structures and vibrational frequencies,¹⁴ but no theoretical data for the NMR spectra are yet available. In particular, the complex $[(NC)_5Pt-Tl(CN)]^-$ (**I**) has been experimentally extensively investigated by multi-nuclear NMR and Raman spectroscopy. The NMR spectra show three magnetically nonequivalent carbons, which we label with A, B, and C.¹⁵ Apart from the very large Tl–Pt spin–spin



coupling of ~ 57 kHz, one of the most remarkable features of the NMR spectrum of **I** is the fact that the two-bond coupling ${}^2J(\text{Tl}-\text{C}^{\text{A}})$ is much larger than the one-bond coupling ${}^1J(\text{Tl}-\text{C}^{\text{B}})$ —provided the structure proposed in ref 13 based on the NMR and Raman spectra is correct. On the basis of our computational results, we will show that the experimentally observed spin–spin coupling pattern for **I** is indeed compatible with the proposed structure, and we will give an explanation for the magnitudes of the experimentally observed coupling constants. Inclusion of charge donation from the solvent (water) and its effect on the couplings, further enhanced by large relativistic effects, is necessary to provide an explanation for the experimentally observed patterns. The solvent effects turn out to be sizable, e.g., increasing the relativistic coupling between Tl and Pt by more than 100%. The σ bonds along the C–Pt–Tl–C axis are rather delocalized, which seems to be of some importance for the coupling constants.

Section 2 deals with some methodological and computational details and introduces several acronyms used in Section 3. In Section 3 we compare computed and experimental molecular structures and spin–spin couplings, and provide an analysis of the data. Concluding remarks are given in Section 4.

2. Methodology and Computational Details

Density functional computations on complex **I** have been carried out with the Amsterdam Density Functional (ADF)

code.¹⁶ The Vosko–Wilk–Nusair (VWN) density functional¹⁷ has been applied to determine unperturbed Kohn–Sham orbitals. We have obtained satisfying results with the VWN functional in previous work concerning heavy metal spin–spin coupling constants.^{8–10} Relativistic geometry optimizations employ the frozen core approximation, using the quasirelativistic method described in ref 18. Indirect nuclear spin–spin coupling constants have been obtained with a program recently developed by us within the ADF program package. It employs the two-component “zeroth order regular approximation” (ZORA) relativistic method¹⁹ to compute couplings involving heavy atoms. Details about theory and implementations are described elsewhere.^{8,9} We would like to note that although the ZORA hyperfine terms are somewhat different from the well-known Fermi-contact (FC), spin-dipole (SD), paramagnetic orbital (PSO), and diamagnetic orbital (DSO) operators of the non-relativistic theory,²⁰ their influence is very similar and allows similar interpretations. We will therefore refer to FC, SD, PSO, and DSO terms throughout this work also when we refer to their ZORA relativistic generalizations. Consult refs 8 and 9 for a more detailed discussion of the differences between the nonrelativistic and the ZORA hyperfine terms. Values for spin–spin coupling constants refer to the ${}^{205}\text{Tl}$, ${}^{195}\text{Pt}$, and ${}^{13}\text{C}$ nuclei. If not stated otherwise, we have omitted the expensive computation of the often very small SD contribution. However, it is included in the spin–spin couplings based on spin–orbit coupled two-component orbitals since its inclusion in these calculations leads only to a marginal increase in computational time.

The frozen core Slater-type basis sets used for geometry optimizations include 5s/p/d and 6s/p as valence shells for Pt and Tl, respectively, while the 1s shell has been kept frozen for C, N, and O. All electron Slater type basis sets, augmented with steep 1s functions in the case of Pt and Tl as described in ref 8, have been used for the computations of spin–spin couplings. All basis sets are of triple- ζ quality + one polarization function (except for Tl) in the valence shells and of double- ζ quality for the core shells in the case of all-electron computations (ADF basis sets “IV”, ref 16).

As in ref 10, graphical representations of orbitals and other functions computed by ADF have been prepared with our ADFPLT program. Localized orbitals were obtained by the Boys and Foster method,²¹ which earlier has been implemented into the ADF code by one of us (J.A.). In addition, the computation of the electron localization function ELF²² has been implemented by us into the ADF auxiliary program DENSF¹⁶ and can be visualized with ADFPLT.

(16) ADF 2.3.3. Theoretical Chemistry, Vrije Universiteit, Amsterdam. ADF 1999.02, Theoretical Chemistry, Vrije Universiteit, Amsterdam, <http://www.scm.com>, see also: te Velde, G.; Baerends, E. J. *J. Comput. Phys.* **1992**, *99*, 84. Fonseca Guerra, C.; Visser, O.; Snijders, J. G.; te Velde, G.; Baerends, E. J. In *Methods and Techniques for Computational Chemistry*; Clementi, E., Corongiu, C., Eds.; STEF: Cagliari, 1995.

(17) Vosko, S. H.; Wilk, L.; Nusair, M. *Can. J. Phys.* **1989**, *58*, 1200.
(18) (a) Ziegler, T.; Tschinke, V.; Baerends, E. J.; Snijders, J. G.; Ravenek, W. *J. Phys. Chem.* **1989**, *93*, 3050. (b) Schreckenbach, G.; Ziegler, T.; Li, J. *Int. J. Quantum Chem.* **1995**, *56*, 477.

(19) (a) Chang, C.; Pelissier, M.; Durand, M. *Phys. Scr.* **1986**, *34*, 394. (b) van Lenthe, E.; Baerends, E. J.; Snijders, J. G. *J. Chem. Phys.* **1993**, *99*, 4597. (c) van Lenthe, E.; Baerends, E. J.; Snijders, J. G. *J. Chem. Phys.* **1994**, *101*, 9783. (d) van Lenthe, E.; van Leeuwen, R.; Baerends, E. J.; Snijders, J. G. *Int. J. Quantum Chem.* **1996**, *57*, 281.

(20) Ramsey, N. F. *Phys. Rev.* **1953**, *91*, 303.
(21) (a) Boys, S. F.; Foster, J. M. *Rev. Mod. Phys.* **1960**, *32*, 300. (b) Boys, S. F. In *Quantum Theory of Atoms, Molecules and the Solid State*; Löwdin, P. O., Ed.; Academic Press: New York, 1966; p 253.

(22) (a) Becke, A. D.; Edgecombe, J. *J. Chem. Phys.* **1990**, *92*, 5397. (b) Savin, A.; Nesper, R.; Wengert, S.; Fässler, T. *Angew. Chem., Int. Ed. Engl.* **1997**, *36*, 1808; *Angew. Chem.* **1997**, *109*, 1892.

(11) (a) Mikkelsen, K. V.; Ruud, K.; Helgaker, T. *J. Comput. Chem.* **1999**, *20*, 1281. (b) Pecul, M.; Sadlej, J. *Chem. Phys.* **1998**, *234*, 111.

(12) Berg, K. E.; Glaser, J.; Read, M. C.; Tóth, I. *J. Am. Chem. Soc.* **1995**, *117*, 7550.

(13) Malariik, M.; Berg, K.; Glaser, J.; Sandström, M.; Tóth, I. *Inorg. Chem.* **1998**, *37*, 2910.

(14) Russo, M. R.; Kaltsoyannis, N. *Inorg. Chim. Acta* **2001**, *312*, 221.

(15) The labeling convention follows the one adopted in refs 12–14.

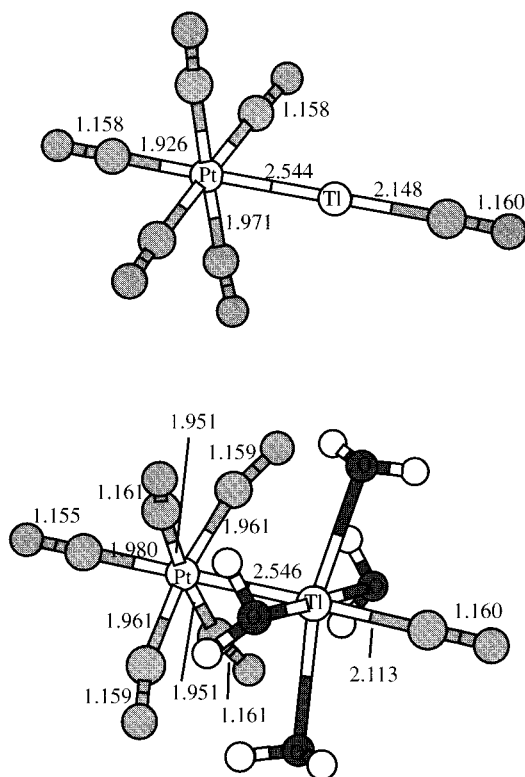


Figure 1. Scalar relativistically optimized structures of complex **I** with and without solvent molecules. All distances in Å. The mean Tl–O distance in the solvated complex is 2.54 Å. Experimentally determined (ref 23) bond distances are the following: Pt–Tl, 2.598; Pt–C^A, 2.01; Tl–C^B, 2.13; C–N, 1.15; Tl–O, ~2.51.

3. Results and Discussion

The structures of complex **I** which have been obtained from scalar relativistic geometry optimizations are displayed in Figure 1. The results are comparable to the ones obtained in ref 14 with the ADF program, employing slightly different basis sets for C, N, and O. Experimentally determined bond lengths from EXAFS spectroscopy in aqueous solution²³ are listed in the caption of Figure 1, too. To simulate the solvated complex, geometry optimizations have been carried out including four water molecules bound to Tl. In ref 23, experimental evidence for such an arrangement is reported. The proposed experimental structure has a Pt–Tl bond length that is slightly longer than the R_e value obtained from the quasirelativistic geometry optimizations.

Table 1 lists the experimentally observed and computed nuclear spin–spin couplings for complex **I**. We have studied the influence of electronic spin–orbit coupling on the computed couplings for the solvated complex as well. Obviously, the coupling constants are not very strongly influenced by the electronic spin–orbit coupling, which allows for a somewhat more intuitive discussion at the scalar relativistic level involving real pure α and β spin orbitals. The overall accuracy of the couplings in comparison with experiment is reasonably good, taking the large solvent effects and the rather simple computational approach of its effects into account. The scalar relativistic increase of the couplings—especially of $^1J(\text{Pt}–\text{Tl})$ —is very substantial. The contributions to the spin–spin couplings due to the electronic orbital angular momentum (PSO and DSO)

Table 1. Spin–Spin Coupling Constants in Complex **I**, in Hertz

coupling ^a	nrel ^b	rel ^c	rel, 4aq ^d	so, 4aq ^e	expt ^f
$^1J(\text{Pt}–\text{Tl})$	5410	18976	43102	40292	57020
$^1J(\text{Tl}–\text{C}^B)$	–1222	–5692	3081	3001	2446
$^2J(\text{Tl}–\text{C}^A)$	3428	5670	7983	7537	9743
$^2J(\text{Tl}–\text{C}^C)^g$	–249	–484	–381	–392	452
$^1J(\text{Pt}–\text{C}^A)$	682	1382	1037	1007	843
$^1J(\text{Pt}–\text{C}^C)^g$	444	890	954	920	821
$^2J(\text{Pt}–\text{C}^B)$	62	151	158	141	200
$^3J(\text{C}^B–\text{C}^A)$	36	39	20	24	30

^a Couplings refer to ^{205}Tl , ^{195}Pt , and ^{13}C . FC + PSO + DSO contribution included in the scalar relativistic computations, SD contribution additionally present in spin–orbit computations. ^b Non-relativistic couplings from scalar relativistically optimized geometry, no solvent. ^c Scalar relativistic couplings from scalar relativistically optimized geometry, no solvent. ^d Scalar relativistically optimized geometry including 4 water molecules. ^e Relativistic spin–orbit computation based on scalar relativistic geometry. ^f Reference 13, sign not determined. ^g Mean value of the four coupling constants.

are negligible at the present level of accuracy and therefore not listed separately. All coupling constants are strongly dominated by the Fermi-contact mechanism (FC, due to the electron spin), which is very sensitive to the well-known relativistic increase of valence s-orbital density at the heavy nuclei. Nevertheless, no qualitative agreement with experiment results from computations on the free molecule. Semiquantitatively correct magnitudes for the spin–spin couplings, and in particular the correct coupling pattern, are obtained by explicit inclusion of solvent molecules. The solvent appears to influence the one-bond Tl–C coupling much stronger than the two-bond coupling. However, from Table 1 it can be seen that most coupling constants undergo rather large changes upon coordination of Tl by solvent molecules, especially if the solvent-coordinated atom or its direct neighbors are involved.

The computational results lead to a first conclusion, viz., that the experimentally proposed structure involving a nonbridged Pt–Tl bond is most likely correct. The calculations are able to reproduce the fact that $^2J(\text{Tl}–\text{C}^A)$ is much larger than $^1J(\text{Tl}–\text{C}^B)$, provided that relativity and solvent effects are taken into account. The increase of the computed Pt–Tl coupling due to the solvent is remarkably large and exceeds the solvent effects we have reported earlier¹⁰ for coordinatively unsaturated Pt and Hg complexes. In this previous work we have analyzed the solvent effect in more detail. It was found that charge donation from the solvent to the heavy metal and into the metal–ligand σ bonds is the dominant factor responsible for a large positive shift of the FC contribution to the coupling. Thereby, solvation seems to be reasonably well described by saturating the first coordination shell with solvent molecules.

A second conclusion can be drawn from the data obtained for the free complex in comparison with the solvated one. In the free complex both $^1J(\text{Tl}–\text{C}^B)$ and $^2J(\text{Tl}–\text{C}^A)$ are of the same magnitude, but different in sign. Charge donation from the solvent shifts both values positively, while the one-bond coupling is much stronger affected than the two-bond coupling. See Figure 2. Finally, both coupling constants are positive, with $^2J(\text{Tl}–\text{C}) \gg ^1J(\text{Tl}–\text{C})$. The opposite sign of the two Tl–C couplings in conjunction with the positive solvent shift is responsible for the counterintuitive experimental outcome.

Nevertheless, the question arises why $^2J(\text{Tl}–\text{C}^A)$ is so large in comparison with the magnitude of $^1J(\text{Tl}–\text{C}^B)$ already in the unsolvated complex. To this end we recall that the Tl–C coupling in $\text{Tl}^{\text{III}}(\text{CN})^{2+}$ is ~15 kHz in aqueous solution.²⁴ Complex **I** has been described¹³ as being composed of a

(23) (a) Jalilvand, F. Doctoral Thesis, Department of Chemistry, Royal Institute of Technology, Stockholm, 2000. (b) Jalilvand, F.; Malariik, M.; Sandström, M.; Mink, J.; Persson, I.; Persson, P.; Tóth, I.; Glaser, J. *Inorg. Chem.* Submitted for publication.

(24) Blixt, J.; Györi, B.; Glaser, J. *J. Am. Chem. Soc.* **1989**, *111*, 7784.

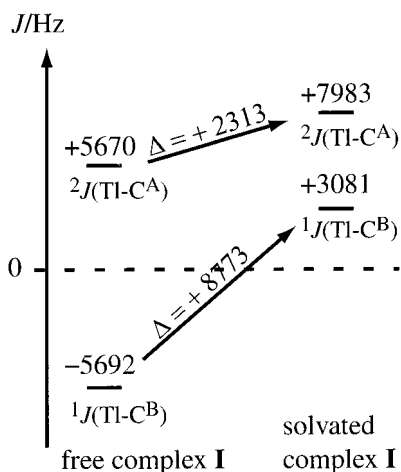


Figure 2. Computed scalar relativistic $^1J(\text{Tl}-\text{C}^B)$ and $^2J(\text{Tl}-\text{C}^A)$ coupling constants including or excluding solvent molecules.

$[\text{Pt}^{\text{II}}(\text{CN})_5]^{3-}$ fragment forming a dative bond to $\text{Tl}^{\text{III}}(\text{CN})^{2+}$, thereby donating charge into the Tl 6s orbital and reducing Tl to a formal oxidation state of <III. Obviously, upon formation of the complex $^1J(\text{Tl}-\text{C}^B)$ undergoes a large negative shift.

From an analysis of the spin–spin coupling constant in terms of individual MO contributions, we are able to identify a few occupied and one virtual σ MO which yield the leading contributions to $^1J(\text{Tl}-\text{C}^B)$ and $^2J(\text{Tl}-\text{C}^A)$, respectively. Neglecting the first-order spin density change induced by the FC operator, the FC contribution to the spin–spin coupling between two nuclei A, B in the nonrelativistic case can be written as²⁵

$$J^{\text{FC}} \propto \sum_i^{\text{occ}} \sum_a^{\text{virt}} \frac{1}{\epsilon_i - \epsilon_a} \cdot \varphi_i \varphi_a |_{\text{Nucleus A}} \cdot \varphi_i \varphi_a |_{\text{Nucleus B}} \quad (1)$$

This equation results from a double first-order perturbation treatment of the molecular energy with respect to the presence of two nuclear spins and is frequently used in experimental and theoretical work for interpretation purposes. The ϵ values are the energies of the real nonrelativistic occupied (occ) and unoccupied (virt, for virtual) Kohn–Sham spin orbitals φ . $\varphi_i \varphi_a |_{\text{Nucleus A}}$ denotes the value of the occupied–virtual orbital product $\varphi_i \varphi_a$ at nucleus A. In the ZORA relativistic case, rather the sign and slope of the orbitals near the nuclei instead of their values at the nuclei have to be considered, but the general interpretation with respect to sign patterns around the nuclei and increase of the FC coupling contribution upon increase of electron density at the nuclei remains similar to eq 1.⁸ An “orbital contribution” arises intuitively (though arbitrarily) from the summation over occupied orbitals φ_i in eq 1.

For the unsolvated complex **I** we find that coupling of occupied σ MOs no. 94, 95, 101, and 114 with a low-lying virtual σ orbital no. 122 (highest occupied MO = HOMO = no. 119) yields the leading contributions to the $\text{Tl}-\text{C}^{A,B}$ couplings. The orbitals are displayed in Figure 3. Table 2 lists their total contributions to the Fermi-contact $\text{Tl}-\text{C}$ couplings, and the partial contributions from the $\varphi_a = \text{no. 122}$ term in eq 1. The listed values include corrections due to the first-order spin density. Two MOs, 95 and 101, and their mixing with virtual MO no. 122 contribute very large values to both $^1J(\text{Tl}-\text{C}^B)$ and $^2J(\text{Tl}-\text{C}^A)$, but with different signs in the case of $^1J(\text{Tl}-\text{C}^B)$. In addition, there is a large contribution from MO 114 to $^1J(\text{Tl}-\text{C}^B)$, which is also negative. The negatively contributing MOs, which determine the sign of $^1J(\text{Tl}-\text{C}^B)$, consist of $\text{Tl}-\text{C}$

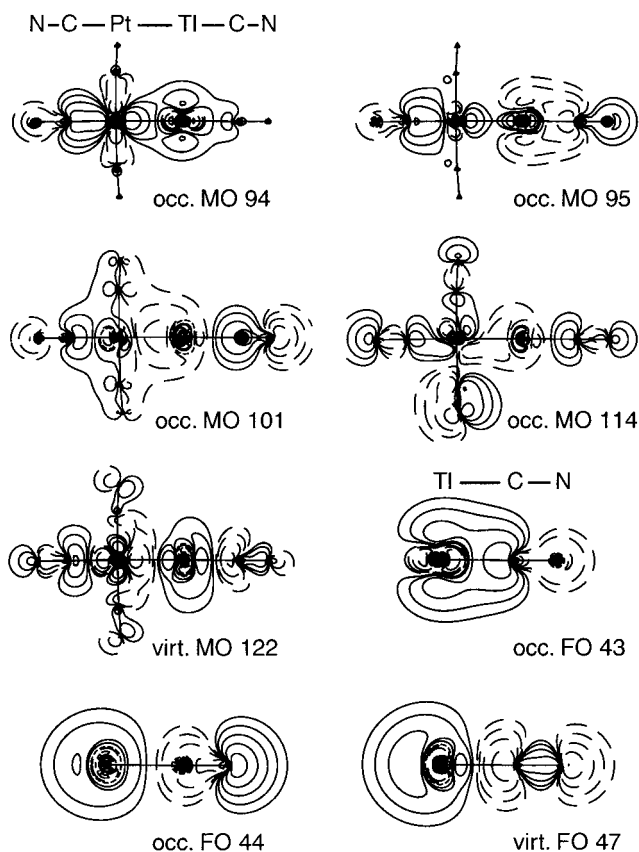


Figure 3. Some scalar ZORA molecular orbitals (MOs) and fragment orbitals (FOs) of the unsolvated complex **I** and the $\text{Tl}(\text{CN})^{2+}$ fragment of complex **I**. The highest occupied MO is no. 119, the highest occupied FO is no. 46. The MOs are plotted in a plane that is spanned by the $\text{C}^A-\text{Pt}-\text{Tl}-\text{C}^B$ axis (left to right) and a $\text{C}^C-\text{Pt}-\text{C}^C$ axis. Contour values are $\pm 0.02 \times 2^n$, $n = 0, 1, 2, \dots$ atomic units ($\sqrt{\text{electrons/bohr}^3}$, 1 bohr $\approx 0.529 \text{ \AA}$); dashed lines indicate negative values.

Table 2. MO Contributions to the $\text{Tl}-\text{C}^{A,B}$ Fermi-Contact Coupling Contribution in the Unsolvated Complex **I**, in Hertz^a

MO no.	$^1J(\text{Tl}-\text{C}^B)$	$^2J(\text{Tl}-\text{C}^A)$
94 total	1101	−3078
94–122	1150	−3985
95 total	6920	3745
95–122	7735	4024
101 total	−9117	4073
101–122	−9390	4381
114 total	−3659	528
114–122	−3471	517
sum	−4755	5268
sum, 122 only	−3976	4937
total calcd ^b	−5661	5672

^a “122” is only the virtual MO no. 122 contribution of eq 1; “total” sums over all virtuals. ^b “Total calcd” is the complete FC contribution to the computed couplings listed in Table 1. The difference between the numbers in this table and in Table 1 is caused by the PSO and the DSO contributions.

antibonding orbitals of a constituting $\text{Tl}(\text{CN})^{2+}$ fragment, one of which (no. 47) is a virtual orbital in $\text{Tl}(\text{CN})^{2+}$ but has an occupation of ~ 1.4 in complex **I**. The fragment orbitals are displayed in Figure 3 as well. Taking only the no. 95, 101, 114, and 122 orbitals into account, the signs of the coupling constants are determined by the sign pattern of these orbitals around the Tl, C^B , and C^A nuclei, respectively. This sign pattern is coupled to the valence shell s-orbital coefficients because of the orthogonality of valence orbitals to the core orbitals, and is therefore determined by the actual bonding situation. To achieve

a positive sign for one of the terms in eq 1, the function $\varphi_i\varphi_a$ has to have different signs at the different nuclei, because $\epsilon_i - \epsilon_a$ is negative for Aufbau configurations. The sign change is achieved, e.g., if $\varphi_i\varphi_a$ is a product of a σ -bonding (like sign at both nuclei) and a σ -antibonding (different sign at the nuclei) orbital. (The situation might be somewhat more complicated for the heavy nuclei due to contributions of the 5s shell to the bond orbitals. In our actual case, the sign patterns of the bond orbitals correspond to the sign patterns of the respective valence 2s and 6s orbital coefficients.) From Figure 3 we can see that MO 95 can be viewed as a combination of a C^A -Pt bonding with a Tl - C^B bonding orbital, 101 and 114 as combinations of a C^A -Pt bonding with Tl - C^B antibonding orbitals, and 122 as a combination of both C^A -Pt and Tl - C^B antibonding orbitals. That MOs 95 and 101/114 contribute with different signs to ${}^1J(Tl-C^B)$ and ${}^2J(Tl-C^A)$ is thereby easily understood by the sign pattern created by the local bonding/antibonding patterns. Since the local antibonding character concerning $Tl-C^B$ is increased by the formation of the complex, compared to the $Tl(CN)_2^{2+}$ fragment, this results in an increasingly negative value of ${}^1J(Tl-C^B)$. The system $Tl(CN)_2^{2+}$ has been measured in aqueous solution. If we assume a comparably strong positive solvent shift for the couplings in $Tl(CN)_2^{2+}$ than for complex **I**, we conclude that not only ${}^2J(Tl-C^A)$ is unexpectedly large in complex **I** but also ${}^1J(Tl-C^B)$ is much more negative than might be expected due to the charge donation of the Pt fragment into $Tl-C^B$ antibonding orbitals upon formation of the complex.

Further insight into the bonding situation in complex **I** emerges from the attempt to localize its orbitals. Orthogonal localized orbitals are obtained here as linear combinations of the canonical²⁶ Kohn-Sham orbitals such as to minimize their mean spatial extension around their center of gravity.²¹ By construction, these localized orbitals yield the same electron density as the canonical orbitals and therefore provide an alternative, equally valid description of bonding. No simple conclusion about the delocalization of bonds can usually be drawn from a visual inspection of the canonical orbitals because they are always delocalized. On the other hand, if a molecule has rather delocalized localized orbitals, it is possible to deduce a delocalized character of the electronic system.²⁷ We find that well-localized two-center bonding orbitals are obtained, e.g., for the CN ligands of complex **I**, while the other localized σ bonding orbitals along the C-Pt-Tl-C axis exhibit substantially larger values at centers further away from the bond partners. Consult Figure 4. An accompanying plot of Becke's "electron localization function" (ELF)²² corroborates this picture. The ELF has been introduced by Becke as a measure of electron localization as a function in 3-dimensional space and has achieved some popularity, e.g., as a tool for the interpretation of structure and electronic properties of inorganic compounds (see, e.g., ref 22b). For complex **I**, ELF stays well below the free electron gas reference value of ELF = 0.5 between Pt and Tl and therefore does not indicate a localized bond between these two atoms (Figure 4). Hence we conclude that complex **I** exhibits delocalized multicenter bonding along the C-Pt-Tl-C axis which cannot be described by one simple Lewis-type

(26) The orbitals which are usually obtained with quantum chemical programs are called "canonical orbitals". They are the eigenfunctions of the Fock operator.

(27) McWeeny, R. *Methods of molecular quantum mechanics*, 2nd ed.; Academic Press: London, 1992.

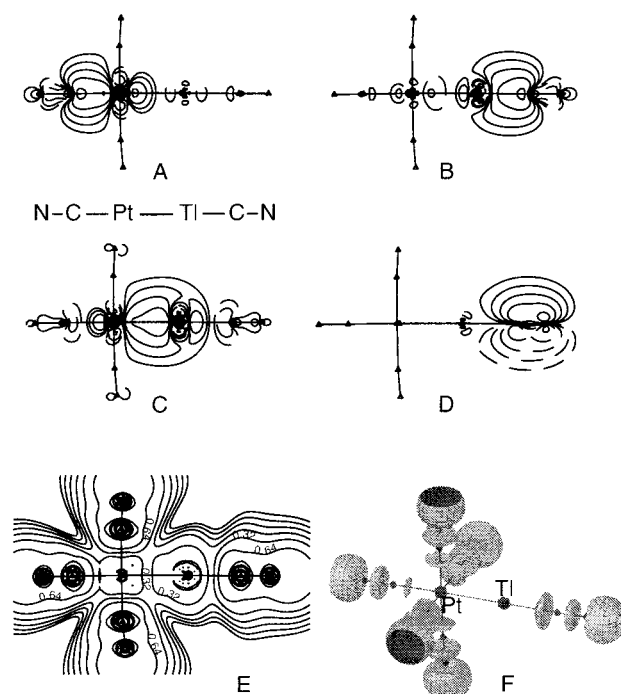


Figure 4. Selected localized orbitals of complex **I**. A, B, C: Somewhat delocalized σ bonds between C^A -Pt, Tl - C^B , and Pt-Tl, respectively. D: A well-localized two-center π bond of a CN ligand. E and F: Electron localization function ELF. ELF = 0.8 for the isosurface plot F. Consult also the caption of Figure 3.

formula. We believe that this multicenter character of the Pt-Tl bond is responsible for the large magnitude of ${}^2J(Tl-C^A)$ in the unsolvated complex. No such multicenter character is found concerning Tl and the four C^C , for which the coupling constants are an order of magnitude smaller as compared to the magnitudes of the $Tl-C^{A,B}$ couplings.

4. Conclusions

We have demonstrated that relativistic density functional calculations are able to reproduce the nuclear spin-spin coupling pattern of complex **I**. Sign and magnitude of the coupling constants are very strongly influenced by the surrounding solvent molecules, which must be taken into consideration in order to obtain a semiquantitatively correct computational answer. In particular, the combination of relativistic effects and a solvent-induced positive shift of the couplings explains why ${}^1J(Pt-Tl)$ is so large and why ${}^2J(Tl-C) \gg {}^1J(Tl-C)$ is observed experimentally. We suggest that solvent effects are generally of great importance for nuclear spin-spin couplings in coordinatively unsaturated complexes containing heavy elements. Interpretations based on spectra obtained from solution should take possible counterintuitive results due to solvent influence into consideration.

Acknowledgment. This work has received financial support from the National Science and Engineering Research Council of Canada (NSERC). We are grateful to Dr. Julius Glaser who has drawn our attention to the interesting title compound and who has provided us with preprints of upcoming manuscripts.

JA003866D